The 2-day wave during the boreal summer of 1994

Dennis M. Riggin,[1] Ruth S. Lieberman,[1] Robert A. Vincent,[2] Alan H. Manson,[3] Christopher E. Meek,[3] Takuji Nakamura,[4] Toshitaka Tsuda,[4] and Yuri I. Portnyagin[5]

[1]   The 2-day wave during the boreal summer of 1994 was observed using stratospheric analyses from the British Met Office and at mesospheric heights using medium-frequency (MF) radars and the microwave limb sounder (MLS) and high-resolution Doppler imager (HRDI) satellite instruments. Most of the evidence from our study points to a high latitude source for the boreal 2-day wave event we observed. We found little evidence for a connection between the 2-day wave event in the mesosphere and activity at lower altitudes. Instead we contend that the 2-day wave observed at upper mesospheric heights was excited in-situ. This event was predominantly zonal wave number 2, was highly localized in time, and the disturbance propagated equatorially from high northern latitudes. At stratopause and lower mesospheric heights the largest 2-day wave amplitudes were seen at high Southern Hemisphere latitudes (i.e., in the winter hemisphere). However, the austral winter 2-day wave was trapped and did not penetrate to upper mesospheric heights.   *INDEX TERMS:* 3334 Meteorology and Atmospheric Dynamics: Middle atmosphere dynamics (0341, 0342); 3360 Meteorology and Atmospheric Dynamics: Remote sensing; 3369 Meteorology and Atmospheric Dynamics: Thermospheric dynamics (0358); 3384 Meteorology and Atmospheric Dynamics: Waves and tides; *KEYWORDS:* 2-day, planetary, wave

1.   Introduction

[2]   The 2-day wave is a highly sporadic planetary wave that is observed with largest amplitudes around (or soon after) summer solstice in the upper mesosphere. During these peak summer periods the 2-day wave can have peak (i.e., zero-to-peak) amplitudes in meridional wind of $\sim$30 m s^{-1} [*Pancheva et al.*, 2004], and peak amplitudes in temperature of $\sim$5 K [*Shepherd et al.*, 1999]. In the MLT the wave typically has long vertical wavelengths of 50– 70 km [*Clark et al.*, 1994; *Palo and Avery*, 1996; *Zhou et al.*, 1997]. As expected for a neutral Rossby wave, the wind perturbations are nearly in phase quadrature with the temperature fluctuations. Nonetheless there can be significant fluxes of heat and constituents associated with the 2-day wave's large amplitudes and high intermittency. The 2-day wave has been intensively studied in a number of multi-instrument observational campaigns (e.g., see *Pancheva et al.* [2004] and references therein). However, most satellite studies have concentrated on the Southern Hemisphere (exceptions are *Wu et al.* [1996], and *Limpasuvan et al.* [2000a]). A number of studies suggest that the Southern Hemisphere 2-day wave is mostly a westward propagating zonal wave number 3 (W3) wave [e.g., *Limpasuvan and Wu*, 2003], although it can include W2 and W4 components [*Lieberman*, 1999]. In the Northern Hemisphere the W4 (and possibly also the W2) component has greater importance [*Meek et al.*, 1996; *Pancheva et al.*, 2004]. Modeling results by *Limpasuvan et al.* [2000b] showed that the weaker summertime jet in the northern stratosphere preferentially excites a W4 component, whose period ($\sim$1.8 days) is shorter than the period ($\sim$2.1 days) of the W3 component. The mixture of components probably contributes to the greater variability in 2-day wave periods that is observed in the Northern Hemisphere [*Thayaparan et al.*, 1997a, 1997b].

[3]   Most studies have also concentrated on either stratospheric or mesospheric heights, and there has been little work attempting to link the 2-day wave in the two regions. In this case study we concentrate on a Northern Hemisphere summer season and compare and contrast the characteristics of the 2-day wave in the mesosphere (as observed by medium-frequency (MF) radars, meteor radar and the microwave limb sounder (MLS) and high-resolution Doppler imager (HRDI) satellite instruments) with the same event in the stratosphere (in UK Meterological Office stratospheric analyses).

[4]   The dual nature of the 2-day wave is now a familiar concept, and the wave is often described as having the character of a normal mode [e.g., *Salby*, 1981; *Randel*, 1994], while at the same time undergoing amplification

[1]Colorado Research Associates, Boulder, Colorado, USA.
[2]Department of Physics and Mathematical Physics, University of Adelaide, South Australia, Australia.
[3]University of Saskatchewan, Institute Space and Atmospheric Studies, Saskatoon, Saskatchewan, Canada.
[4]Radio Science Center for Space and Atmosphere, Kyoto University, Kyoto, Japan.
[5]Institute for Experimental Meteorology, Obninsk, Russia.

due to instability of the summertime, lower-mesospheric, westward jet [e.g., *Fritts et al.*, 1999; *Lieberman*, 1999; *Salby and Callaghan*, 2001]. According to *Pfister* [1985] the dominant instability mechanism is baroclinic, and it operates on the poleward edge of the jet around 50–60°N. Alternatively, *Orsalini et al.* [1997] proposed a low latitude 2-day wave source arising in the summer subtropics on the basis of UK Meterological Office stratospheric analyses. The stratospheric analyses showed that baratropically unstable conditions can be created by inertial instability. As described in the following sections, most of the evidence from our study points to a high latitude source for the boreal 2-day wave event we observed. However, it is likely that the wave has multiple sources.

[5] In section 2 the data sources and analysis methodology are described. The background conditions and potential for instability are assessed in section 3. Observations of the 2-day wave are shown in section 4, and the findings are further discussed and summarized in section 5.

2. Data Sources and Analysis Methodology

[6] The satellite data used for our study comes from two instruments among the suite of instruments on the Upper Atmosphere Research Satellite (UARS), launched in late 1991. The satellite completes ∼14 orbits a day, precessing ∼20 min from day-to-day. The Microwave Limb Sounder (MLS) scans naturally occurring O_2 emissions in the microwave from the stratospheric limb. Our results were obtained using the improved v5 data set described by *Livesey et al.* [2003], and *Wu et al.* [2003]. Temperatures are retrieved on 12 constant pressure surfaces 46–0.01 hPa (∼20–80 km) with reasonable sensitivity. Temperatures were retrieved on additional levels up to 1×10^{-4} hPa. However, wave amplitudes were progressively weaker above 0.01 hPa, and so we did not make use of the upper levels. MLS samples twice per day with a latitude resolution of ∼10° and a height resolution of ∼5 km. The latitude coverage is restricted to 34°S–80°N or 80°S–34°N, depending on the yaw position of the satellite. During the boreal summer 1994 period discussed in this paper, MLS was looking toward the southern (winter) hemisphere. MLS operated May 27–June 21 and August 7–August 27, so there was a long data gap during much of the summer.

[7] The High Resolution Doppler Interferometer (HRDI) is another instrument on the the UARS platform. HRDI retrieves daytime winds and temperatures over the vertical range of 60–110 km by determining the Doppler shift of absorption and emission lines in the O_2 atmospheric band. HRDI vector winds are derived from upward and downward scanned pairs of line-of-sight radiance profiles, viewed from two nearly orthogonal directions. The two tangent points can be made nearly coincident in space, and due to the rapid orbital motion of the satellite (essentially north-south), are only slightly offset in time. The effective latitudinal resolution of the measurements is ∼10°, and the height resolution ∼5 km. During much of HRDI's operating life it viewed the mesosphere or stratosphere on alternate days, a sampling which precludes resolving waves with periods shorter than ∼4 days. However, during several HRDI special observing cam-

paigns the instrument viewed the mesosphere continuously for ∼10 days. The HRDI data presented in this paper are from the last of these campaigns, carried out from July 25 to August 3, 1994. In fact the availability of HRDI data was a major reason 1994 was selected as the year for our case study of the boreal summer 2-day wave. This short period unfortunately does not overlap with the periods of MLS observation noted above. We will show HRDI meridional winds, the only component that unambiguously resolved the 2-day wave during the campaign period.

[8] The 2-day wave perturbation fields were extracted from the MLS and HRDI data fields using a space-time Fourier transform method carried out in satellite relative coordinates. This so-called asynoptic mapping technique was introduced by *Salby* [1982a, 1982b], and derives the perturbation temporal/zonal wave number global-scale fields without any a priori information about the waves present. Because the potential for tidal aliasing is much greater in the mesosphere, double node retrievals are needed to differentiate the different wave components. During this campaign HRDI viewed the limb from sunlit ("warm side") and dark ("cold side") of the spacecraft alternately over 14 orbits, a sampling pattern that restricted the waves that could be resolved to those with zonal wave numbers of four or less. The warm side descending and cold side descending sampling pattern yielded retrievals at 5 latitudes over 0–40°N. *Lieberman and Riggin* [1997] give a physical description of how the technique is applied to satellite data, and show ground tracks for the July 25–August 3, 1994 campaign period. A few additional details (e.g., UARS orbital parameters) are mentioned by *Lieberman et al.* [2003].

[9] The radar data analyzed in this paper were obtained from three medium frequency (MF) radars, and two meteor scatter radars. The MF radars are located at Saskatoon, Canada (52°N, 107°W), Kauai, Hawaii (22°N, 159°W), Christmas Island (2°N, 157°W). The meteor scatter radars are located at Obninsk, Russia (55°N, 37°E) and Jakarta, Indonesia (6°S, 108°E). Both MF and meteor-scatter radars make continuous measurements of the winds with ∼4 km height resolution in the 70–100 km height region. MF radars operate at frequencies near 2 MHz and obtain partial reflection returns from mesospheric ionization. The echoes are received by spatially separated antennas and analyzed using full-correlation analysis (the so-called spaced antenna drift technique) [*Holdsworth and Reid*, 1995]. The MF radars measure winds from 78 to 98 km with the highest data rate around 90 km. More complete descriptions of the MF radar systems at Hawaii and Christmas Island can be found in *Fritts and Isler* [1992] and *Vincent and Lessicar* [1991]. The Jakarta meteor wind radar operates at a frequency near 32 MHz. It measures winds over an altitude range of 70–120 km with a maximum data rate around 90 km. The Jakarta radar uses the Doppler technique with spatially separated antennas and an algorithm for determining the location of meteor echoes. The use of echolocation provides more accurate wind estimates, and makes it possible to use a wide beam which captures more meteor echoes. Even with this enhancement, meteor scatter radars typically have a lower data

rate than partial reflection radars over the heights where both types of systems provide data. A more complete description of the Jakarta radar system is provided by *Tsuda et al.* [1995]. The Obninsk meteor radar operates at 33.3 MHz. During the summer of 1994 the system had no ranging, but most echoes can be assumed to come from 90 to 95 km.

[10] Temporal variations in radar winds are examined using the *S*-transform method, a technique for temporal localization of the Fourier transform [*Stockwell and Lowe*, 2001]. The *S*-transform has an absolute phase reference and collapses in the time domain to give the Fourier spectrum exactly. The amplitudes are easily interpreted since they are the same as would be derived from least squares fits of sinusoids over Gaussian windows. The Gaussian localizing function length is proportional to wave period with a standard deviation equal to the wave period. The standard deviation of a Gaussian is where the peak value falls to ~61% of the maximum, and the window falls to half its peak value at ~1.18 standard deviations. The *S*-transform has an adjustable factor that can be used to increase the frequency resolution at the expense of temporal resolution. Frequency resolution was deemed to be important in our case so this factor was set to three, yielding a half-amplitude temporal resolution of ~14 days for an *S*-transform representation of the 2-day wave. The *S*-transform is conceptually similar to the Morlet wavelet, but in a simple implementation it provides better frequency resolution, since the natural units are linear in frequency as opposed to logarithmic in frequency for the Morlet wavelet.

[11] The zonal mean atmospheric background conditions and 2-day wave characteristics at stratopause heights and below were studied using data assimilations provided by the United Kingdom Meteorological Office. The assimilation model data sets [*Swinbank and O'Neill*, 1994; *Coy and Swinbank*, 1997], are comprised of daily, 3-dimensional fields of temperature, geopotential height, and wind component. These analyses are usually called UKMO, but we will refer to them as Met Office analyses (METO data for short). The horizontal resolution is 2.5° latitude by 3.75° longitude, and data are reported on 22 pressure levels ranging from 1000 hPa to 0.3 hPa (~0–56 km). The METO data sets were constructed mainly from NOAA polar orbiting meteorological satellite observations of temperature, and are independent of any observations made by UARS instruments. The vertical resolution of METO data in the upper stratosphere is limited by the deep vertical weighting function of retrievals from the Stratospheric Sounding Unit (SSU) instrument on the NOAA satellites. In the upper stratosphere, the satellite data were assimilated in vertical layers at 0.4–1 hPa (~48–55 km) and 1–2 hPa (~42–48 km).

[12] The 2-day wave was extracted from the METO fields using a 2-dimensional frequency domain filter. At each time step during 1994, the zonal mean of u, v, and T was subtracted to yield perturbation quantities u′, v′, and T′. A fast Fourier transform (FFT) in longitude and time was applied to the perturbation fields. A window was applied to the frequency domain representations with the desired zonal wave number (W3 or W4) and a tapered passband in the frequency domain with unattenuated periods between 2.0 and 2.4 days. The resulting 1-D

filtered field was then inverse FFT'ed back to the time domain. Of course, there is some aliasing of the 2-day wave field in the daily METO fields. However, were able to verify that the wave variance near the nyquist frequency was predominantly due to westward propagating waves by examination of the 2-D (temporal versus spatial frequency) power spectra.

3. Background Conditions

[13] The dispersion relation for Rossby planetary wave in the quasi-geostrophic beta-plane framework can be written in terms of vertical wave number (m) as

$$m^2 = \frac{N^2}{f_0^2} \left[\frac{\beta}{\bar{u} - c_x} - (k^2 + l^2) \right] - \frac{1}{4H^2} \quad (1)$$

where N is the buoyancy frequency, $f_0 \equiv 2\Omega \sin(\theta)$ is the planetary vorticity, $\beta \equiv 2\Omega \cos(\theta)/a$, ($m$, k, l) are wave numbers in the vertical zonal and meridional direction, respectively, H is the scale height, c_x is the ground-based phase speed, and $\bar{u}$ is the zonal mean zonal wind. The period of the 2-day wave is normally between 2 and 2.2 days. Although the period during an event does fluctuate (as will be shown later in the radar observations), to first order the phase speed ($c_x = \omega_0/k$) can be considered to vary only due to the geometric dependence of k on latitude. A Rossby wave vertically propagates when $m^2 > 0$, and when $m^2 < 0$ the wave is vertically evanescent. The condition $\bar{u} \to c_x$ (i.e, a westward $\bar{u}$ approaching the wave phase speed) corresponds physically to a shrinking vertical wavelength and a critical layer. Conversely, a large positive (eastward) $\bar{u}$ yields a a large vertical wavelength, and if large enough, wave reflection.

[14] Instability of $\bar{u}$ can be diagnosed with the meridional gradient of zonally averaged vorticity,

$$\frac{\partial \bar{Q}}{\partial y} = \beta - \frac{1}{a^2} \frac{\partial}{\partial \phi} \left[\frac{1}{\cos\phi} \frac{\partial}{\partial \phi} (\bar{u} \cos\phi) \right] - \frac{1}{\rho_0} \frac{\partial}{\partial z*} \left[\rho_0 \frac{f^2}{N^2} \frac{\partial \bar{u}}{\partial z*} \right] \quad (2)$$

where $z* \equiv -H \ln(p/p_s)$ is the scaled pressure height. If $\partial \bar{Q}/\partial y < 0$, the flow will be unstable to perturbations. The terms of (2) involving $\partial/\partial \phi$ and $\partial/\partial z*$ can be loosely described as barotropic and baroclinic contributions to instability, respectively. Over the height range 30–56 km where we will apply (2), $H \simeq 7$ km (corresponding to a 240 K isothermal atmosphere), $N \simeq 0.02$ s^{-1}, and both parameters are relatively constant. Thus the last term of (2) can be approximated as

$$\frac{1}{\rho_0} \frac{\partial}{\partial z*} \left[\rho_0 \frac{f^2}{N^2} \frac{\partial \bar{u}}{\partial z*} \right] = \frac{f^2}{N^2} \left[-\frac{1}{H} \frac{\partial \bar{u}}{\partial z*} + \frac{\partial^2 \bar{u}}{\partial z*^2} \right] \quad (3)$$

[15] Figure 1 shows monthly averaged latitude-height cross sections of the mean wind during 1994 from METO data. The shading denotes regions where $\partial \bar{Q}/\partial y$ is negative as defined by (2). The critical layer for a hypothetical 2-day wave is denoted with heavy black dots. The phase speed of this hypothetical wave was defined by fixing the period at 2.2 days with a W3 horizontal scale.
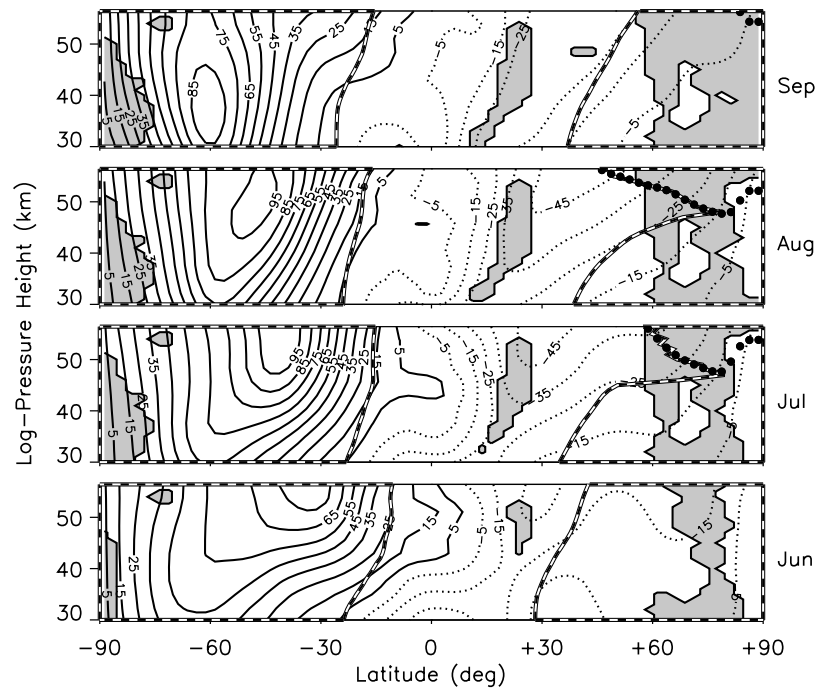
Figure 1. Monthly averages of $\overline{u}$ from METO data. The gray shading defines regions where $\partial\overline{Q}/\partial y < 0$. The heavy black dots show a hypothetical 2-day wave critical line (see text fordetails), and the heavy dashed line outlines regions where $m^2 < 0$ as calculated from (1).

The critical layer does not appear until July, penetrates southward during August and then retreats during September. The critical layer lies within a region of negative $\partial\overline{Q}/\partial y$. A wave will strongly interact and exchange energy with the mean flow along the critical line. Although this critical line interaction is usually considered to cause damping of the wave, the unstable configuration of $\overline{u}$ can cause the critical line to act as a wave source [*Salby and Callaghan*, 2001]. The rather sudden appearance of this hypothetical wave source around 60°N suggests a connection with the seasonal occurrence of the 2-day wave. The baroclinic term and barotropic terms
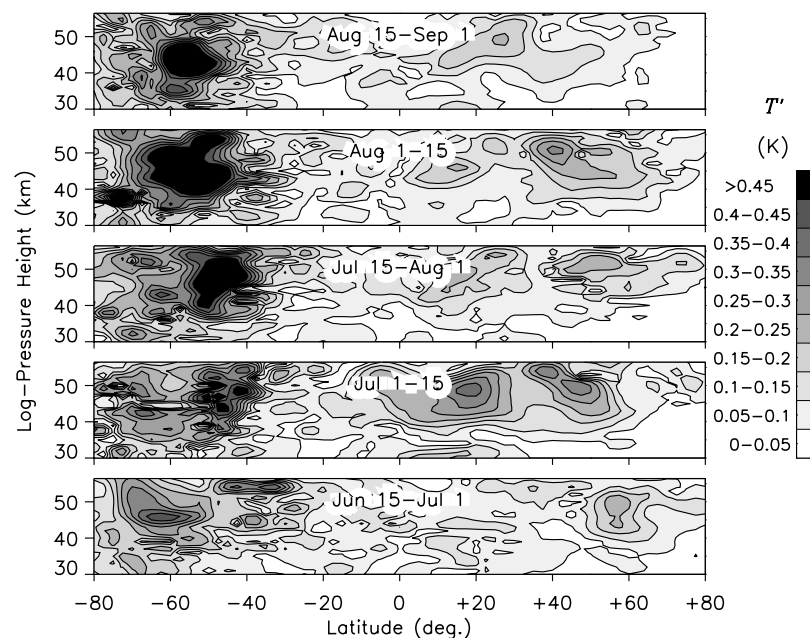

Figure 2. Perturbation temperature amplitudes from METO data for the W3 component with periods of 2.0–2.4 days. The panels show consecutive 15-day time averages (time increasing upward).
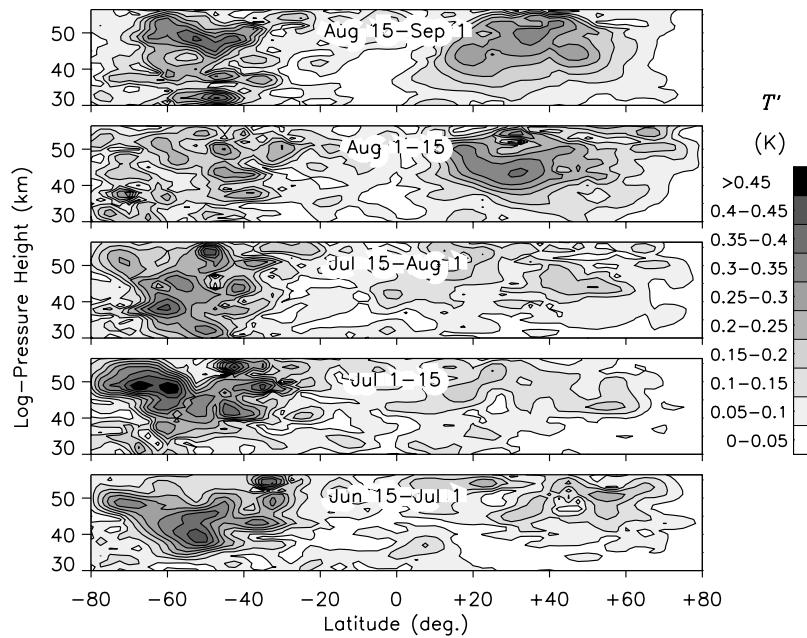
Figure 3. Same as Figure 2, but for the W4 component.

of (2) were found to be of comparable importance in producing the region of negative $\partial \overline{Q}/\partial y$ along the critical line in Figure 1. The heavy dashed line in Figure 1 defines regions of negative m^2 (wave evanescence) as calculated from (1). This calculation is based on the same

hypothetical wave parameters used to define the critical layer. It should be noted that the wave is not necessarily excluded from the $m^2 < 0$ regions since a ray emanating from a wave source will in general propagate meridionally as well as vertically. However, direct vertical
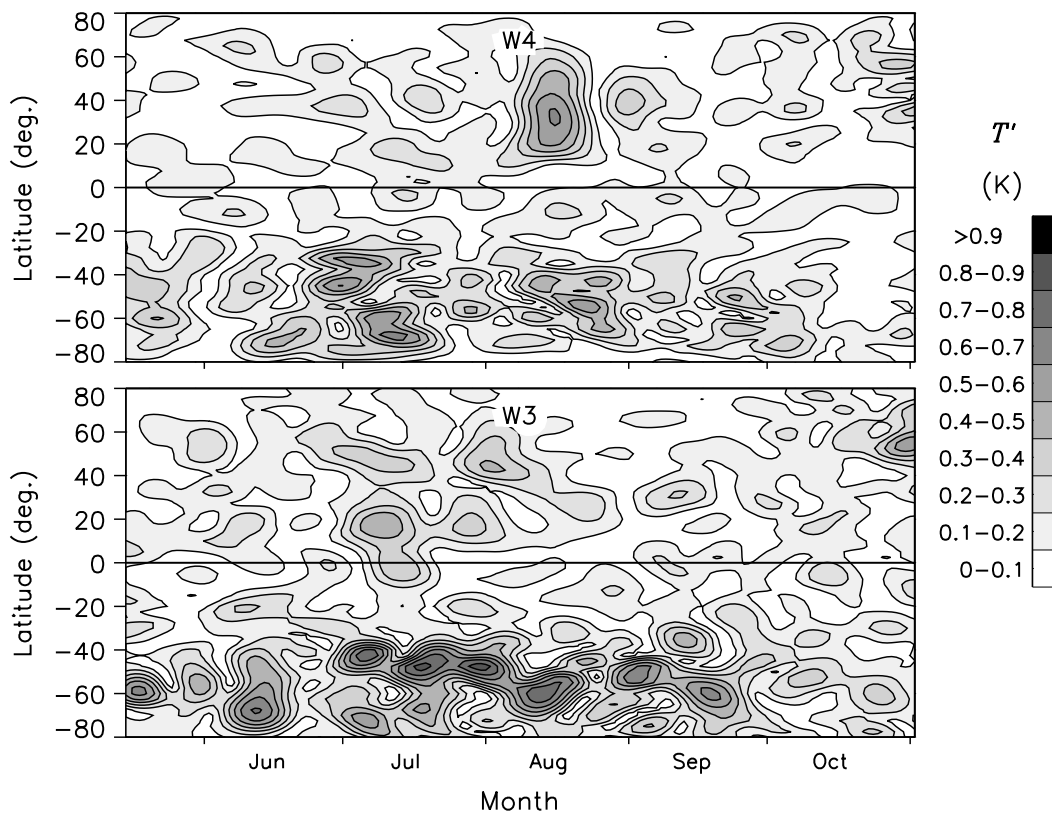

Figure 4. Contours of METO perturbation temperature amplitudes at the 1 hPa pressure level with periods of 2.0–2.4 days. W3 component is shown in the lower panel and W4 in the upper panel.
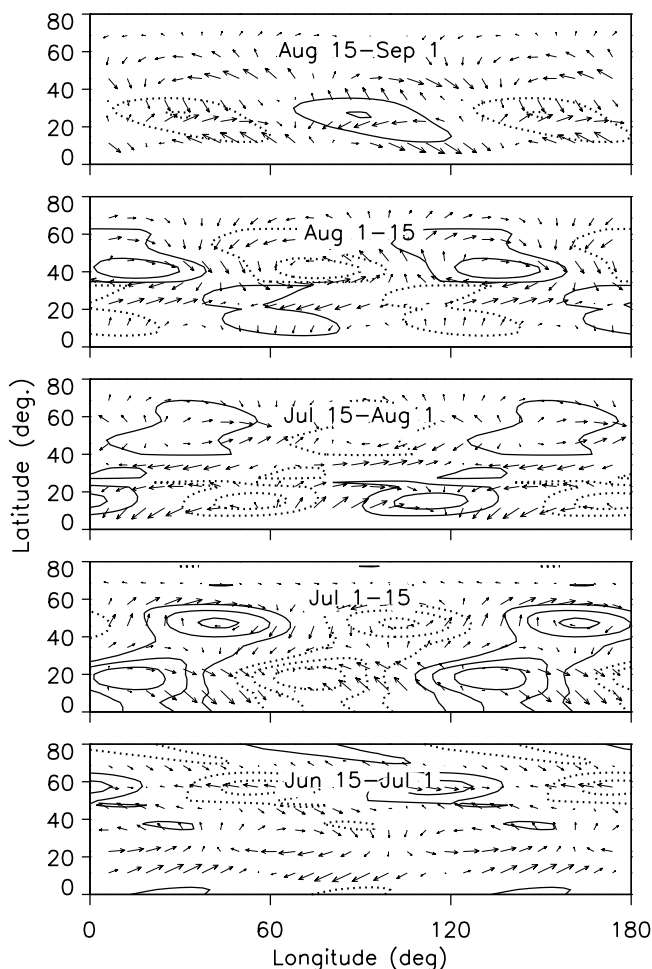
Figure 5. Mapped METO temperature contours and wind vectors for the W3 component with periods of 2.0–2.4 days on the 1 hPa pressure level. The temperature contour increments are 0.1 K (zero contour not drawn), the negative temperature contours are dotted, and the longest wind vectors correspond to a velocity of ~1 m s^{-1}. The mappings are two-week time averages over consecutive periods (time increasing upward).

propagation is permitted only in the latitude band of ~20°S–50°N. Besides the region of negative $\partial \overline{Q}/\partial y$ at 60°N there are unstable regions around 20°N and at high southern latitudes. However, these other pockets of instability do not extend to the top of the grid. Although the 2-day wave excited at high southern latitudes is trapped, unstable regions at these latitudes might be sources for the eastward propagating 4-day wave in the mesosphere [*Coy et al.*, 2003].

4. Observations

[16] Figure 1 established a plausible source for the 2-day wave, and we now look for evidence that the wave was actually present. Performing a two-dimensional (longitude-time) FFT on the METO temperature field we can extract a zonal wave number of choice (W3 or W4) and periods of 2.0–2.4 days. Figure 2 shows the wave perturbation

temperature for W3. The largest amplitudes are in the Southern Hemisphere, although the wave is likely to be trapped here, as suggested by the highly localized vertical structure. In the Northern Hemisphere the largest W3 two-day wave amplitudes are during July 1–15. The Northern Hemisphere W3 wave shows up in two regions at ~25°N and ~60°N that roughly correspond to the localized regions of negative $\partial \overline{Q}/\partial y$ in Figure 1. The W4 component of the 2-day wave, shown in Figure 3 is less localized in latitude in the Northern Hemisphere than the W3 component and it peaks later during August 1–15. *Lieberman* [1999] described the W3 and W4 components of the 2-day wave as forming a "packet," in that they have nearly matching phase speeds. The METO data provides only daily samples, so the 2-day wave is poorly resolved in frequency. However, spectral representations (not shown) of the 2-day wave in METO data show more aliasing for the W4 component, suggesting a shorter period.

[17] The 2-day wave signal is generally largest in the METO data around the 1 hPa pressure level (~48 km). The distribution of the the signal in latitude in time can be derived by taking a 2-D FFT of the temperature at this
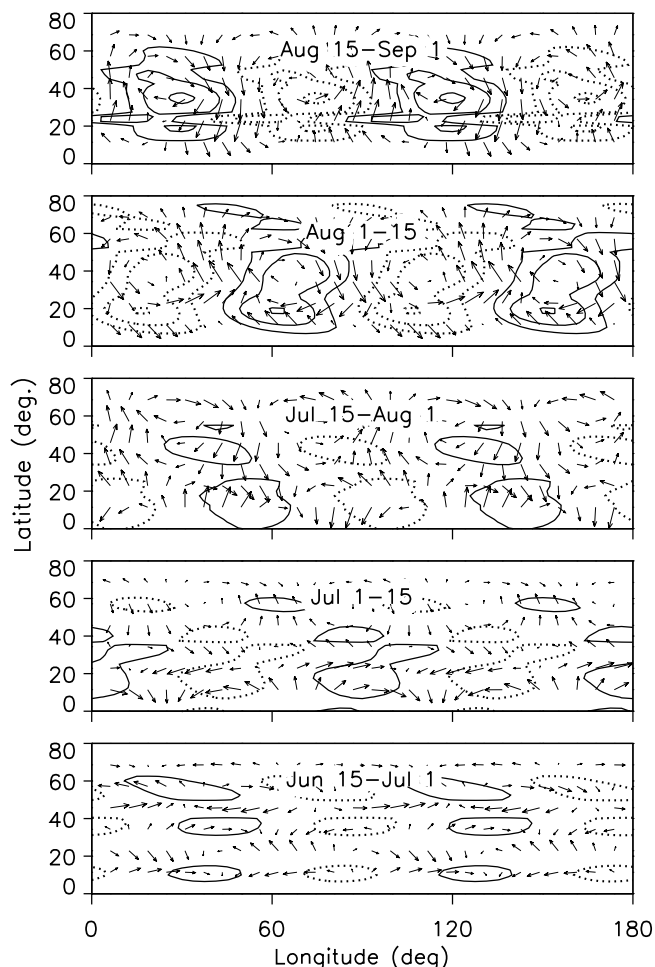

Figure 6. Same as Figure 5, but for the W4 2-day wave component. The longest wind vectors correspond to a velocity of ~1.7 m s^{-1}. The mappings are two-week time averages over consecutive periods (time increasing upward).
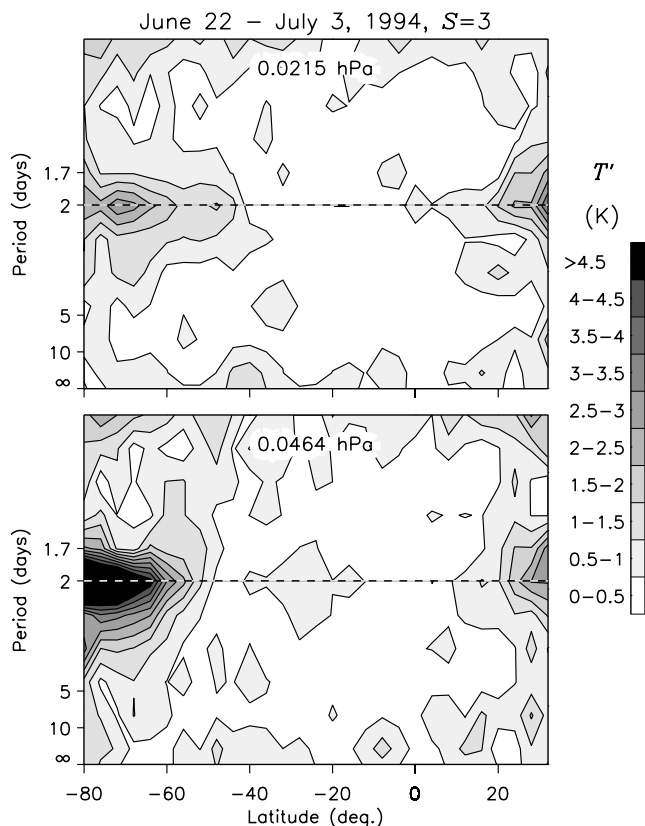
Figure 7. Spectrogram of westward propagating W3 temperature perturbations as seen by MLS at two consecutive pressure levels, 0.464 hPa (~72 km) and 0.215 hPa (~76 km).

~50°N that are offset in phase by ~20° longitude. They appear to coincide with the two regions of negative $\partial \overline{Q} / \partial y$ identified in Figure 1. The W4 component of the 2-day wave, shown in Figure 6, has temperature perturbations with a broader latitudinal extent and occurred later in the summer after the W3 component has died away. The maximum perturbation winds associated with the W4 component (~1.7 m s^{-1}) are considerably stronger than those associated with the W3 component (~1 m s^{-1}). Both the W3 and W4 components tilt eastward with increasing latitude during the periods when the wave components are strong which may indicate northward phase propagation.

[19] Figures 7 and 8 show spectrograms derived from MLS data of temperature perturbation amplitude for W3 and W4, respectively on constant pressure surfaces. The lower panels are at the 0.0464 hPa pressure level (~72 km), and the upper panels are at 0.0215 hPa (~76 km). Only the westward propagating part of the spectrograms are shown. The spectral amplitudes were obtained by performing Salby analysis on temperatures collected between June 22 and July 3, 1994. The MLS instrument was in a southern hemisphere viewing yaw during this period, but the 2-day wave can been seen near the northward edge of the grid at 32°N. The W3 component shown in Figure 7 peaks at a period of two days. In the lower panel of Figure 7, corresponding to a pressure of 0.0464 hPa or ~72 km, there is a huge (~9 K) 2-day amplitude peak in the southern hemisphere poleward of ~60°S. The strong trapping of the Southern Hemisphere wave can be seen in the drastic

pressure level and then extracting the W3 and W4 components with periods of 2.0–2.4 days from the daily METO data. The W3 amplitudes shown in the bottom panel of Figure 4 are much larger in the Southern Hemisphere, but some enhanced activity is visible during July and early August in the northern hemisphere. The W4 activity, shown in the upper panel of Figure 4, is much better defined and is delayed until mid-August.

[18] Mappings of the winds and temperatures from the METO data provide further insight into the 2-day wave structure near the stratopause. The 2-day wave is highly variable from day-to-day, so some averaging is needed to produce mappings that are representative. Figure 5 shows mappings of the W3 2-day wave component averaged over 15 days. During the June 15–July 1 period (bottom map in Figure 5), the wave is restricted in latitude to around 60°N. The amplitude maximizes during July 1–15 and a second amplitude maximum appears around 20°N that is shifted westward. The largest amplitudes are during the July 1–15 period (second map from the bottom), and subsequently the wave decays. The perturbations are rather weak near the stratopause, although the amplitudes have been reduced by the 15 day averaging. The pattern is fairly neutral (i.e., geostrophic) with a cyclonic wind circulation around the cold perturbations. The temperature regions are also quite localized in latitude so the wave fluxes little heat meridionally. There are two regions of wave activity at ~20°N and
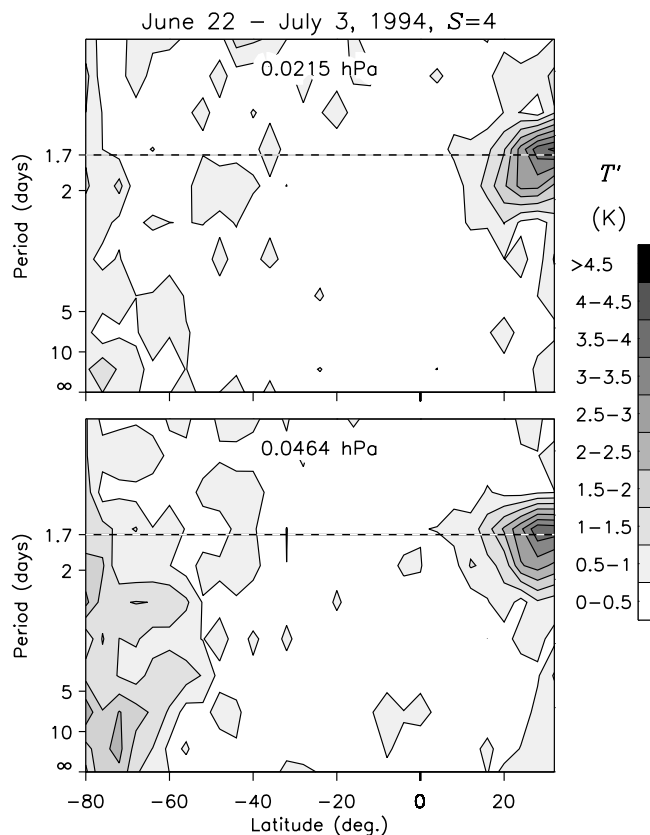

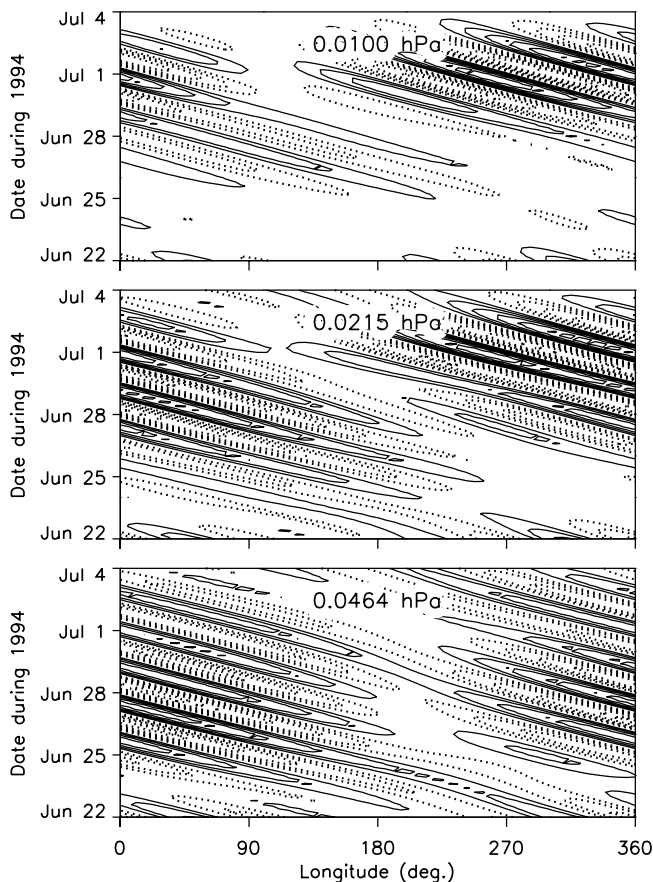**Figure 8.** Same presentation of MLS data as Figure 7, but for W4.

Figure 9. Hövmoller diagrams of the 2-day wave temperature perturbations seen by MLS at 32°N. The three panels show successive pressure levels (increasing upward) that correspond to heights of ~72 km, 76 km, and 80 km. Solid (dotted) lines are positive (negative) temperature perturbations. The contour increment is 2 K, and the 0 K contour has been omitted.

reduction in wave amplitude at the next pressure level of 0.0215 hPa (~76 km). In contrast, the Northern Hemisphere 2-day perturbation is nearly constant between these two pressure levels. At higher heights the 2-day perturbation in MLS data gradually decreases in amplitude. We are unsure to what extent the amplitude decrease is an artifact the retrieval, but it should be noted that MLS temperature perturbations at all wavelengths and periods drop precipitously at the uppermost pressure levels. In the northern hemisphere, the W4 2-day wave, (shown in Figure 8) is somewhat larger than the W3 component, but the W4 2-day wave is entirely absent from the Southern Hemisphere.

[20] The MLS perturbation temperature field resulting from the superposition of the W3 and W4 components of the 2-day wave can be viewed with a Hövmoller diagram (longitude versus time plot). Figure 9 shows the field reconstructed from the 12 day sequence starting on June 22, 1994. The W3 contribution includes wave periods of 1.47–3.14 days, and the W4 contribution includes 1.44–3.03 days. Figure 9 reveals that the phase velocities of the W3 and W4 components are closely matched. The superposition of two different zonal wave numbers leads to relatively

strong perturbation amplitudes around 0° longitude and weaker perturbations around 200° longitude where the zonal wave numbers interfere destructively. Owing to the phase locking, this longitudinal pattern persists through the 12 days of observations. As height increases, the perturbations are delayed to the latter part of the observing period.

[21] Figure 10 shows S-transforms of the meridional wind at multiple radar sites arranged from high to low latitude (top to bottom). Note that the Obninsk radar operated only during the early part of the summer and there is also missing data at Jakarta (white bands). The S-transform amplitudes at each height available between 84 and 94 km have been averaged together in this representation. The contour intervals are 2 m s^{-1} and the frequency axes are logarithmic. A dashed line is drawn across each of the panels with a period of two days. Figure 10 shows a clear evolution of the 2-day wave activity in time and latitude. The early onset of the wave at Obninsk (55°N) suggests that a high-latitude source for the 2-day wave. At Saskatoon the wave has a bifurcated structure with distinct peaks at periods longer and shorter than 2 days. At lower latitudes the onset of 2-day wave activity is progressively delayed, but there are obvious similarities in the 2-day wave signal. Continuity in the time of onset of 2-day wave activity is seen all the way to Jakarta (6°S), although there is considerable wave activity here that is not correlated with the other sites. It should be noted that Jakarta tends to be much more geophysically noisy than Christmas Island, probably due to its location in the western Pacific "warm pool" (e.g., see *Riggin et al.* [1997]). The S-transforms of the zonal wind field shown in Figure 11 show weak amplitudes at the low latitude radar sites and lack the clear progression in time and latitude seen in the meridional component. This wind pattern is consistent with the Hough mode structure of the third Rossby-gravity (3,0) normal mode often associated with the 2-day wave (see Introduction). In theory this mode has a structure with wind gyres centered on the equator, so that the flow is predominantly meridional at low latitudes and closes zonally at high latitudes.

[22] We now examine HRDI fields reconstructed from the 10-day sequence that began on July 25, 1994. Figure 12 shows W2 spectral amplitudes of the meridional wind field at four heights. The signature of the 2-day wave is clear and strong in the meridional wind field, but in the zonal wind and temperature fields (not shown) a 2-day wave signature is either absent or confused by the presence of other wave peaks. Some of the aliased wave peaks appear to be associated with a strong ultra-fast Kelvin wave that has been studied using this same 10 days of HRDI observations [*Lieberman and Riggin*, 1997]. The largest 2-day wave amplitudes were observed at 80 km. The dominant zonal wave number component of the 2-day wave was overwhelmingly W2. However, small W3 and W4 2-day wave peaks were seen at 30°N as shown in Figure 13.

[23] Using spectral information we can can map the HRDI meridional wind into a Hövmoller digram, like the one shown in Figure 9 for the MLS temperature field. Figure 14 shows reconstructions for a height of 80 km. The 10° and 20°N latitude panels were derived from the W2 fluctuations with periods of ~1.4–4.0 days, and the panel at 30° was derived from a combination of zonal wave numbers W2, W3, and W4 over the same band of wave period. The timing of the 2-day wave event seen by HRDI in Figure 14
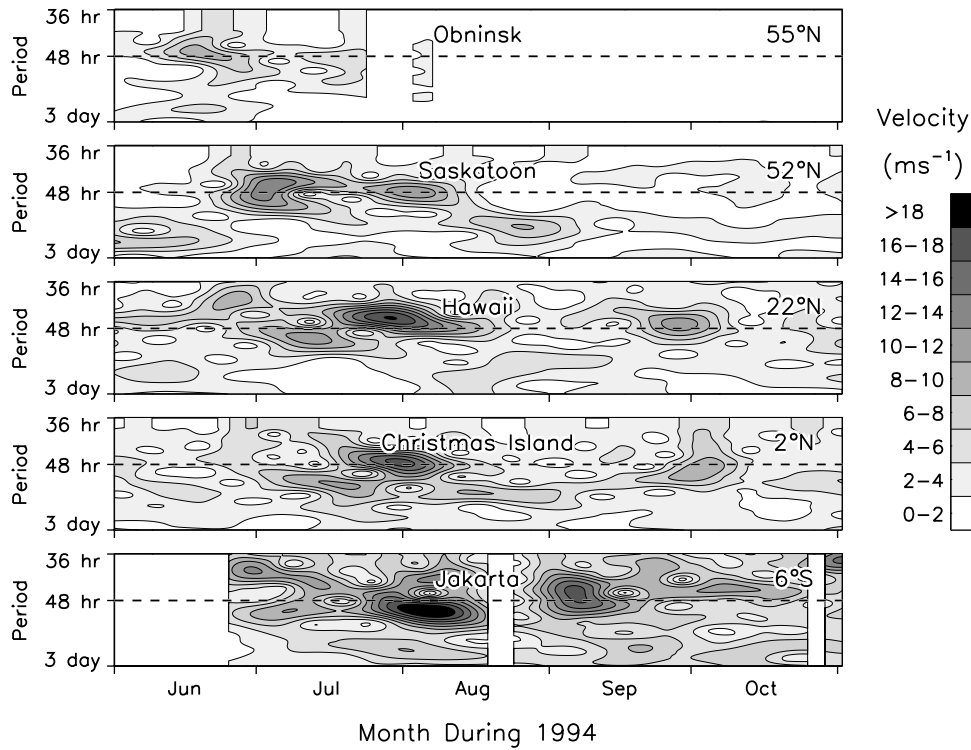
Figure 10. *S*-transform representation of the meridional wind arranged by latitude (see label in the right-hand of each panel).

shows some consistency with the event as seen by the radars in Figure 10. Both figures shows some tendency for the onset of the event to be delayed at lower latitudes. At the latitude of Hawaii (~20°N) the time of onset is late July in

both the MF radar and HRDI observations. Figure 15 shows a detailed comparison of the two instruments. The top panel shows HRDI 2-day wave meridional winds reconstructed from the HRDI W2 spectrum, while the bottom panel shows
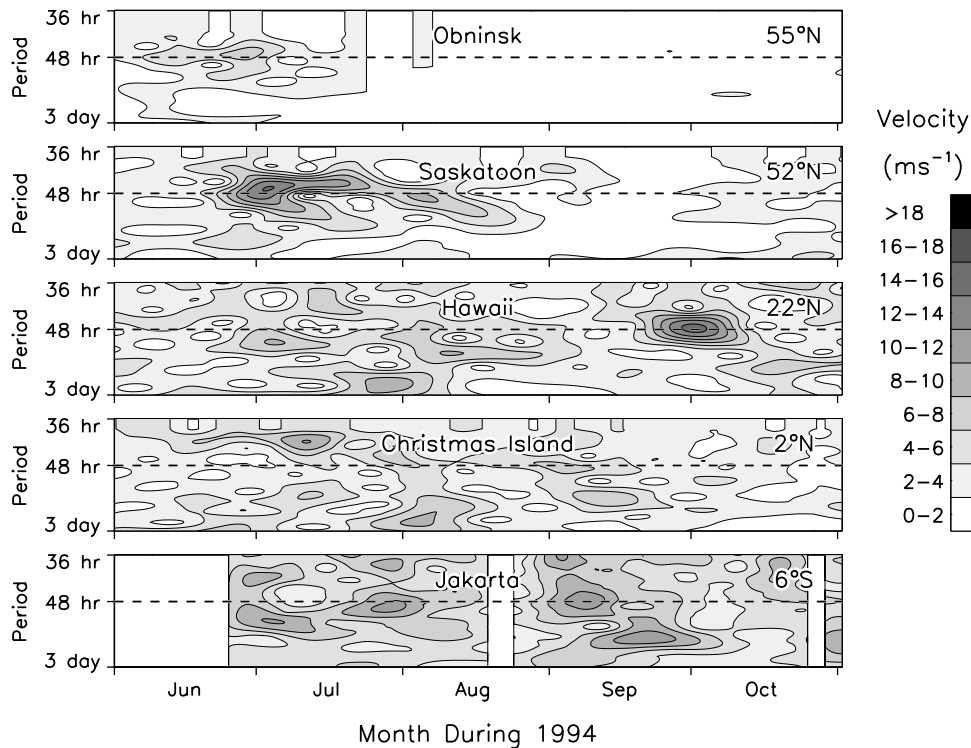

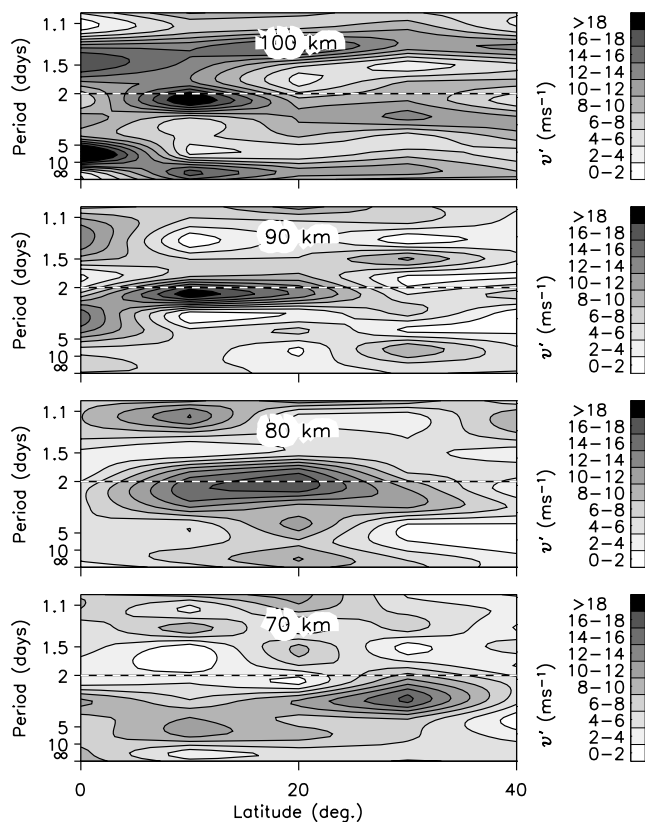**Figure 11.** Same as Figure 10, but for the zonal wind component.

Figure 12. Spectral amplitude of HRDI W2 meridional velocity fluctuations as a function of latitude for the July 25–August 3, 1994 observing period.

winds from the Hawaii MF radar. The diurnal tide was quite large in the radar meridional wind field, but has been removed from Figure 15 by subtracting a composite and then bandpass filtering between 1.5 and 4 days. The details of the HRDI and radar representations of the 2-day wave are different. This isn't too surprising since the HRDI representation is formed from the asynoptic sampling spectrum that includes all longitudes and then applying a phase value that is appropriate for the longitude of Hawaii. On the other hand there are similarities between the 2-day wave as viewed by the two instruments. The perturbation is comparable in amplitude ($\sim$40 m s^{-1} peak), the perturbation is strongly localized in height, and the height at which the perturbation maximizes gradually moves up in height during the 10 days of observation. The vertical wavelength of the 2-day wave is $\sim$40 km in both data sets.

5. Discussion

[24] A motivation for combining data from the stratosphere (METO and MLS) with data from the mesosphere (HRDI and MF radar) was to look for evidence of coupling between regions. Modeling studies by *Salby and Callaghan*, [2001] suggest that the characteristics of the 2-day wave in the mesosphere reflect those in the upper stratosphere. According to this picture, the wave receives auxiliary forcing from instability of the mesospheric jet, but maintains the period and structure it had in the stratosphere. In

contrast we found little evidence for a connection between the 2-day wave event in the mesosphere and activity at lower altitudes. However, there is some ambiguity in this interpretation because the two satellite data sets we analyzed (MLS and HRDI) were quite brief ($\sim$10 days) and did not overlap in time. It should also be mentioned that the boreal summer of 1994 was probably atypical in regard to 2-day wave activity. In a climatology of the 2-day wave in MLS temperatures *Limpasuvan et al.* [2000a] found weak amplitudes during mid-1994 compared to other years. On the basis of our observations we contend that the 2-day wave we observed in mesosphere did not propagate from below, but instead was excited in-situ. This conclusion is supported by the localization of the perturbation in height (see Figures 12 and 15), and the different wave number composition compared with lower heights. At heights near the stratopause the 2-day wave was composed of W3 and W4 components with no evidence of any W2 contribution. Conversely, the 2-day wave in HRDI meridional winds was dominated by the W2 component. The MLS temperatures might have expected to show all three zonal wave numbers because these measurements spanned the stratosphere and the mesosphere up to $\sim$80 km with reasonable sensitivity. However, our analysis of the MLS data segment (June 22–July 3, 1994) revealed no trace of a W2 component. Probably the W2 component observed by HRDI during July 25–August 3, 1994 developed later in the summer. The agreement between HRDI and the Hawaii
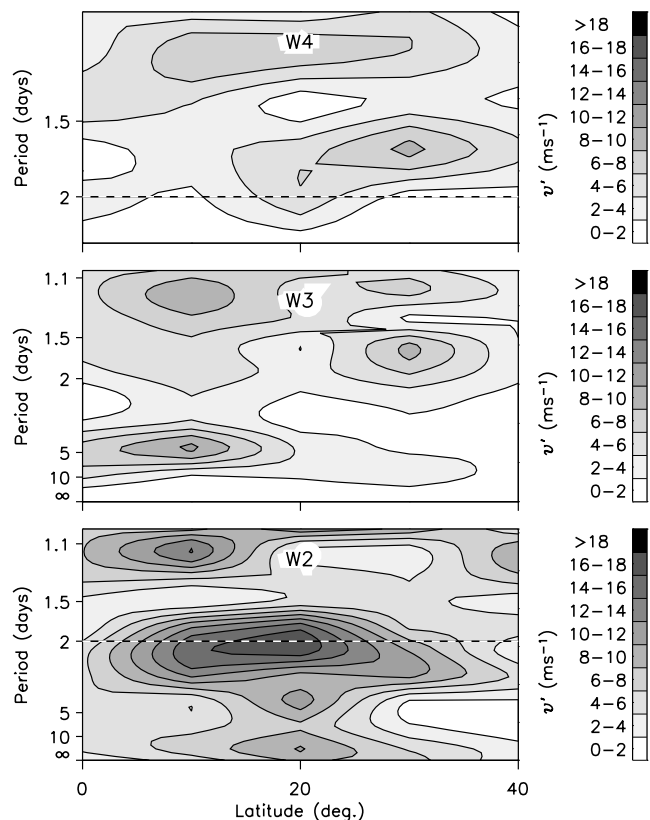

Figure 13. Spectral amplitude of HRDI meridional velocity fluctuations as a function of latitude and period at a height of 80 km. The three panels are different zonal wave numbers.
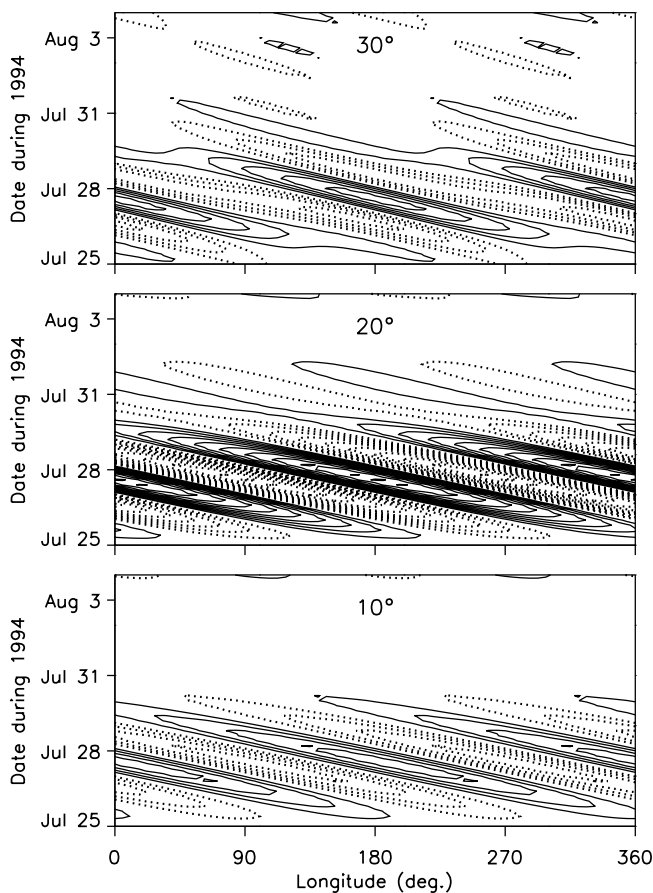
Figure 14. Hövmoller diagrams of HRDI meridional wind fluctuations at a height of 80 km. The three panels show different latitudes north of the equator. Solid (dotted) lines are positive (negative) velocity perturbations. The contour increment is 10 m s^{-1}, and the 0 m s^{-1} contour has been omitted.

MF radar meridional wind measurements in Figure 15 suggest that the Hawaii radar was mostly seeing this W2 component. However, the dominant wave period seen by the Hawaii MF during this time was shorter than two days (see Figure 10), which implies a higher zonal phase speed than normally attributed to the 2-day wave. On the basis of Figure 10, the W2 perturbation traveled from north to south at a group speed of ∼1.5 m s^{-1}, while moving upward (based on Figure 15) at a speed of ∼0.2 m s^{-1}.

[25] The existence of a 2-day wave in the winter mesosphere has received little mention in the literature. During the boreal winter the wave has been reported in mesospheric wind measurements by the WINDII instrument aboard the UARS satellite [*Ward et al.*, 1996], as well as several radars at mid-to-high latitudes [*Manson et al.*, 2004a, 2004b; *Nozawa et al.*, 2003]. There is anecdotal evidence that the 2-day wave may be less prevalent in austral winter as compared to boreal winter. Poleward of 40°S in the austral winter stratosphere we saw nearly continuous 2-day W3 and W4 wave activity from June through September 1994 in the METO temperature data at heights from 30 km to the stratopause. The 2-day wave activity in the winter hemisphere was concentrated in "pockets" that were highly

localized in height (e.g., see Figures 2 and 11). We interpret this height localization as due to vertical trapping of the wave (discussed earlier in conjunction with Figure 1). A winter hemisphere 2-day wave was also observed in MLS temperatures at heights up to ∼72 km (only in the W3 component at this height). Making a hemispheric comparison, the 2-day wave was weaker in the northern (summer) hemisphere in both METO and MLS data. In the northern (summer) hemisphere, the W3 component had significant amplitudes during July and August. The W4 component was stronger, but was confined to the month of August (see Figure 4). Figure 1 established that the seasonal appearance of the boreal 2-day wave was consistent with the development of unstable background conditions. The key factors appear to have been a 2-day wave critical line cutting through a region of $\partial \overline{Q} / \partial y$.

[26] Although the W4 component of the 2-day wave is not a normal mode, it (along with the W3 component) has the character of a normal mode. Figures 5 and 6 show the circulation associated with the components to be quasi-geostrophic, i.e., the wind vectors are parallel to the temperature contours. The maximum stratospheric E-P fluxes computed from the combined W3 and W4 components in the METO data were found to be extremely weak (∼1 × 10^{-3} m s^{-1}day^{-1}). The W3 and W4 2-day wave components have been described as forming an unstable packet [e.g., *Lieberman and Riggin*, 1997]. This is true in the sense that the two components were locked to the same phase speed (see Figure 9). However, this description is somewhat misleading (or at least an over simplification) in our case because the W3 and W4 components appeared at different times and had different latitudinal structures (as shown by Figure 4).
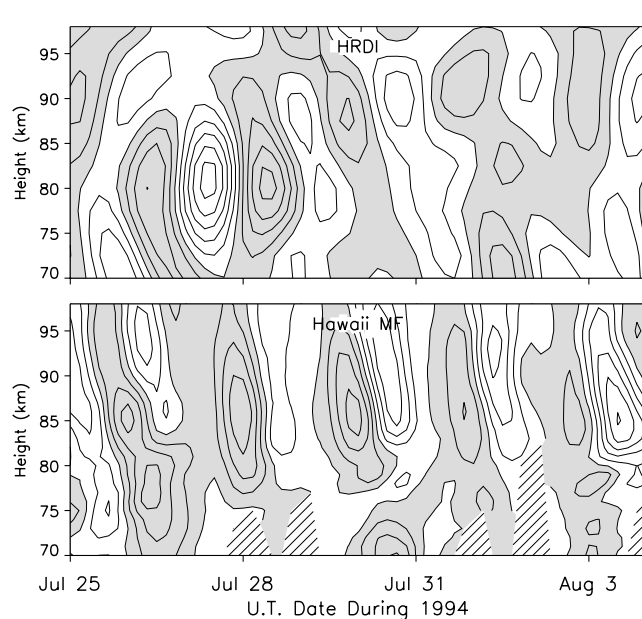

Figure 15. Height-time variation of 2-day wave meridional winds from HRDI data for the longitude of Hawaii (top). Two-day wave meridional winds from the Hawaii MF radar (bottom). The contour interval is 10 m s^{-1} and negative velocities are shaded. Cross-hatch in the lower panel denotes missing data.

[27] In summary, the 2-day wave is a complicated phenomenon, with seemingly independent sources in the northern and southern hemispheres and also with separate sources in the stratosphere and mesosphere. This complexity makes the 2-day wave difficult to analyze and model and our study has mainly been confined to documenting the 2-day wave's characteristics during a particular season. Further multi-instrument studies are needed to assess whether the behavior we observed was representative of other years or unusual.

References

Clark, R. R., A. C. Current, A. H. Manson, C. E. Meek, S. K. Avery, S. E. Palo, and T. Aso (1994), Hemispheric properties of the 2-day wave from mesosphere-lower thermosphere radar observations, *J. Atmos. Sol. Terr. Phys.*, *56*, 1279–1288.

Coy, L., and R. Swinbank (1997), Characteristics of stratospheric winds and temperatures produced by data assimilation, *J. Geophys. Res.*, *102*, 25,763–25,781.

Coy, L., I. Štainer, A. M. DaSilva, J. Joiner, R. B. Hood, S. Pawson, and S. J. Lin (2003), High-frequency planetary waves in the polar middle atmosphere as seen in a data assimilation system, *J. Atmos. Sci.*, *60*, 2975–2992.

Fritts, D. C., and J. R. Isler (1992), First observations of mesospheric dynamics with a partial reflection radar in Hawaii (22°N, 160°W), *Res. Lett.*, *19*, 409–412.

Fritts, D. C., J. R. Isler, R. S. Lieberman, M. D. Burrage, D. R. Marsh, T. Nakamura, T. Tsuda, R. A. Vincent, and I. M. Reid (1999), Two-day wave structure and mean-flow interactions observed by radar and HRDI, *J. Geophys. Res.*, *104*, 3953–3969.

Holdsworth, D. A., and I. M. Reid (1995), A simple model of atmospheric radar backscatter: Description and application to the full correlation analysis of spaced antenna data, *Radio Sci.*, *30*, 1263–1280.

Lieberman, R. S. (1999), Eliassen-Palm fluxes of the 2-day wave, *J. Atmos. Sci.*, *56*, 2846–2861.

Lieberman, R. S., and D. Riggin (1997), High resolution Doppler imager observations of Kelvin waves in the equatorial mesophere and lower thermosphere, *J. Geophys. Res.*, *102*, 26,117–26,130.

Lieberman, R. S., D. M. Riggin, S. J. Franke, A. H. Manson, C. Meek, T. Nakamura, T. Tsuda, R. A. Vincent, and I. Reid (2003), The 6.5-day wave in the mesosphere and lower thermosphere: Evidence for baroclinic/barotropic instability, *J. Geophys. Res.*, *108*(D20), 4640, doi:10.1029/2002JD003349.

Limpasuvan, V., and D. L. Wu (2003), Two-day observations of UARS Microwave Limb Sounder mesospheric water vapor and temperature, *J. Geophys. Res.*, *108*(D10), 4307, doi:10.1029/2002JD002903.

Limpasuvan, V., C. B. Leovy, and Y. J. Orsolini (2000a), Observed temperature 2-day wave and its relatives near the stratopause, *J. Atmos. Sci.*, *57*, 1689–1701.

Limpasuvan, V., C. B. Leovy, Y. J. Orsolini, and B. A. Boville (2000b), A numerical simulation of the 2-day wave near the stratopause, *J. Atmos. Sci.*, *57*, 1702–1717.

Livesey, N. J., W. G. Read, L. Froidevaux, J. W. Waters, H. C. Pumphrey, D. L. Wu, M. L. Santee, Z. Shippony, and R. F. Jarnot (2003), The UARS Microwave Limb Sounder version 5 data set: Theory, characterization and validation, *J. Geophys. Res.*, *108*(D13), 4378, doi:10.1029/2002JD002273.

Manson, A. H., et al. (2004a), Longitudinal and latitudinal variations in dynamic characteristics of the MLT (70–95km): A study involving the CUJO network, *Ann. Geophys.*, *22*, 347–365.

Manson, A. H., C. E. Meek, C. M. Hall, S. Nozawa, N. J. Mitchell, D. Pancheva, W. Singer, and P. Hoffmann (2004b), Mesopause dynamics from the scandinavian triangle of radars within the PSMOS-DATAR Project, *Ann. Geophys.*, *22*, 367–386.

Meek, C. E., et al. (1996), Global study of Northern Hemisphere quasi-2-day wave events in recent summers near 90 km altitude, *J. Atmos. Sol. Terr. Phys.*, *58*, 1401–1411.

Nozawa, S., S. Imaida, A. Brekke, C. M. Hall, A. Manson, C. Meek, S. Oyama, K. Dobashi, and R. Fujii (2003), The quasi 2-day wave observed in the polar mesosphere, *J. Geophys. Res.*, *108*(D2), 4039, doi:10.1029/2002JD002440.

Orsalini, Y. J., V. Limpasuvan, and C. B. Leovy (1997), The tropical stratopause in the UKMO stratospheric analyses: Evidence for a 2-day wave and inertial circulations, *Q. J. R. Meteorol. Soc.*, *123*, 1707–1724.

Palo, S. E., and S. K. Avery (1996), Observations of the quasi 2-day wave in the middle and lower atmosphere over Christmas Island, *J. Geophys. Res.*, *101*, 12,833–12,846.

Pancheva, D., et al. (2004), Variability of the Quasi-2-Day Wave Observed in the MLT Region during PSMOS Campaign of June–August 1999, *J. Atmos. Sol. Terr. Phys*, in press.

Pfister, L. (1985), Baroclinic instability of easterly jets with applications to the summer mesopause, *J. Atmos. Sci.*, *42*, 313–330.

Randel, W. J. (1994), Observations of the 2-day wave in NMC stratospheric analyses, *J. Atmos. Sci.*, *51*, 306–313.

Riggin, D. M., D. C. Fritts, T. Tsuda, T. Nakamura, and R. A. Vincent (1997), Radar observations of a 3-day Kelvin wave in the equatorial mesosphere, *J. Geophys. Res.*, *102*, 26,141–26,157.

Salby, M. L. (1981), The 2-day wave in the middle atmosphere: Observations and theory, *J. Geophys. Res.*, *86*, 9654–9660.

Salby, M. L. (1982a), Sampling theory for asynoptic satellite observations. Part I: Space-time spectra, resolution, and aliasing, *J. Atmos. Sci.*, *39*, 2577–2601.

Salby, M. L. (1982b), Sampling theory for asynoptic satellite observations. Part II: Fast Fourier synoptic mapping, *J. Atmos. Sci.*, *39*, 2601–2614.

Salby, M. L., and P. F. Callaghan (2001), Seasonal amplification of the 2-day wave: Relationship between normal mode and instability, *J. Atmos. Sci.*, *58*, 1858–1869.

Shepherd, M. G., W. E. Ward, B. Prawirosoehardjo, R. G. Roble, S.-P. Zhang, and D. Y. Wang (1999), Planetary scale and tidal perturbations in mesospheric temperature observed by WINDII, *Earth Planet. Space*, *51*, 593–610.

Stockwell, R. G., and R. P. Lowe (2001), Airglow Imaging of Gravity Waves. Part I: Results from a small network of OH Nightglow Scanning Imagers, *J. Geophys. Res.*, *106*, 17,185–17,203.

Swinbank, R., and A. O'Neill (1994), *A stratosphere-troposphere data assimilation scheme*, *Mon. Weather Rev.*, *122*, 686–702.

Thayaparan, T., W. K. Hocking, and J. MacDougall (1997a), Amplitude, phase and period variations of the quasi-2-day wave in the mesosphere and lower thermosphere over London, Canada (43°N, 81°W), during 1993 and 1994, *J. Geophys. Res.*, *102*, 9461–9478.

Thayaparan, T., W. K. Hocking, J. MacDougall, A. H. Manson, and C. E. Meek (1997b), Simultaneous observations of the 2-day wave at London (43°N, 81°W) and Saskatoon (52°N, 107°W) near 91 km during the two years of 1993 and 1994, *Ann. Geophys.*, *15*, 1324–1339.

Tsuda, T., et al. (1995), A preliminary report on observations of equatorial atmospheric dynamics in Indonesia with radars and radiosondes, *J. Meteorol. Soc. Jpn.*, *73*, 393–406.

Vincent, R. A., and D. Lessicar (1991), Dynamics of the equatorial mesosphere: First results with a new generation of partial reflection radar, *Geophys. Res. Lett.*, *18*, 825–828.

Ward, W. E., D. Y. Wang, B. H. Solheim, and G. G. Shepherd (1996), Observations of the 2-day wave in WINDII data during January, 1993, *Geophys. Res. Lett.*, *23*, 2923–2926.

Wu, D. L., E. F. Fishbein, W. G. Read, and J. W. Waters (1996), Excitation and evolution of the quasi-2-day wave observed in UARS/MLS temperature measurements, *J. Atmos. Sci.*, *53*, 728–738.

Wu, D. L., et al. (2003), Mesospheric temperature from UARS MLS: Retrieval and validation, *J. Atmos. Sol. Terr. Phys.*, *65*, 245–267.

Zhou, Q. H., M. P. Sulzer, and C. A. Tepley (1997), An analysis of tidal and planetary waves in the neutral winds and temperature observed at low-latitude E region heights, *J. Geophys. Res.*, *102*, 11,491–11,505.

————————————

R. S. Lieberman and D. M. Riggin, Colorado Research Associates Division, NorthWest Research Associates, Inc., 3380 Mitchell Lane, Boulder, CO 80301, USA. (riggin@colorado-research.com; ruth@colorado-research.com)

A. H. Manson and C. E. Meek, University of Saskatchewan, Institute Space and Atmospheric Studies, 116 Science Place, Saskatoon, Saskatchewan, Canada S7N 5E2. (manson@dansas.usask.ca; meek@dansas.usask.ca)

T. Nakamura and T. Tsuda, Radio Science Center for Space and Atmosphere, Kyoto University, Gokasho, Uji, Kyoto 611-0011, Japan. (nakamura@kurasc.kyoto-u.ac.jp; tsuda@kurasc.kyoto-u.ac.jp)

Y. Portnyagin, Scientific Production Association "Typhoon" Institute for Experimental Meteorology, Obninsk 249020, Russia. (yportgin@typhoon.obninsk.org)

R. A. Vincent, Department of Physics and Mathematical Physics, University of Adelaide, S. A. 5005, Australia. (rvincent@physics.adelaide.edu.au)